J. Phys. Chem. Lett. 2022, 13, 7320–7335. https://doi.org/10.1021/acs.jpclett.2c01776

Interpretation of the Recombination Lifetime in Halide Perovskite Devices by Correlated Techniques

Juan Bisquert*

[1] Institute of Advanced Materials (INAM), Universitat Jaume I, 12006 Castelló, Spain.

[2]Yonsei Frontier Lab, Yonsei University, Seoul 03722, South Korea.

Corresponding author (bisquert@uji.es)

Abstract

The recombination lifetime is a central quantity of optoelectronic devices, as it controls properties such as the open-circuit voltage and light emission rates. Recently the lifetime properties of halide perovskite devices have been measured over a wide range of the photovoltage, using techniques associated to a steady state by small perturbation methods. It has been remarked that observation of the lifetime is affected by different additional properties of the device such as multiple trapping and capacitive charging. We discuss the meaning of delay factors in the observations of recombination lifetime in halide perovskites. We formulate a general equivalent circuit model that is a basis for the interpretation of all the small perturbation techniques. We discuss the connection of the recombination model to the previous reports of impedance spectroscopy (IS) of halide perovskites. Finally we comment the correlation properties of the different light-modulated techniques.

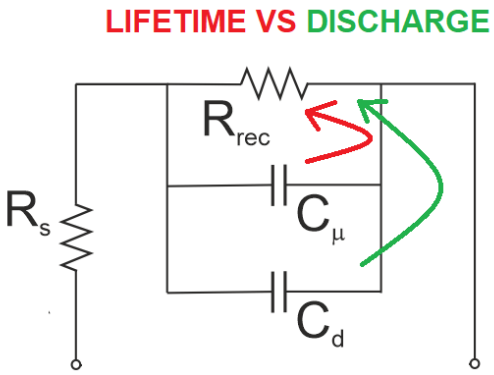

Juan Bisquert is a professor of Applied Physics at Universitat Jaume I de Castelló. He is the funding director of the Institute of Advanced Materials. He published the book **Physics of Solar Energy Conversion** (CRC Press 2020) that establishes a general physical picture of solar energy devices. He has been distinguished in the list of Highly Cited Researchers from 2014 to 2021. He is Executive Editor for Europe of the Journal of Physical Chemistry Letters. His research activity is dedicated to the mechanisms of energy devices as the hybrid metal halide perovskites, a class of photovoltaic materials and devices that show excellent performance. He also investigates the resistive switching of perovskites for memory applications and brain-inspired computing.

Quotes

There is, therefore, a significant opportunity to conciliate different methods to obtain a robust set of system parameters.

a main criterion to obtain a recombination lifetime in homogeneous conditions is the clear observation of the chemical capacitance,

A correlation of different methods that was realized for organic and silicon solar cells has not been established so far for halide perovskites.

The recombination lifetime τ_{rec} is a central quantity to the analysis of semiconductor optoelectronic devices such as solar cells. τ_{rec} is the time for recombination of injected or photogenerated electrons and holes.[1] The measured lifetime may be associated to a single microscopic mechanism or correspond to a composition of them such as band-to-band radiative recombination and Shockley-Read-Hall defect-mediated nonradiative recombination.[2,3]

The electronic carrier lifetimes in a material can be investigated by optical stimulation of a contactless film, that contains only the light absorber material over a substrate, using a range of time-resolved optical techniques including transient absorption spectroscopy (TAS), optical-pump-terahertz-probe (OPTP), time-resolved-microwave-conductivity (TRMC), time-resolved-photoluminescence (TRPL), time-resolved-2D-Fourier-transformed-infrared spectroscopy (TR-2D-FTIR) and other techniques.

However, one is generally interested to obtain the lifetimes in working devices with contacts. The optical methods are still useful tools, probably with different results due to the additional properties introduced by the electrodes such as interface induced recombination. In addition for a full device it is possible to measure the electrical quantities of current and voltage, and a new set of methods to determine lifetimes appears. The recombination parameters may be established by purely stationary techniques, such as obtaining the ideality factor of the exponentially raising current dependence on voltage.[4,5] But a number of time and frequency resolved methods provide more direct information on the required kinetic parameters.

There are two types of such "dynamic" methods. We may establish a large perturbation and observe the decay to equilibrium, as in the open-circuit voltage, V_{oc}, decay (OCVD) that provides the lifetime over a wide voltage range with a single measurement.[6,7] Sometimes large signal techniques are the method of choice, as in the measurement of the current-voltage curve. It is also beneficial that with one measurement you can get information on different mechanisms. However, the parameters change strongly in the course of the measurement, when the lifetime is concentration or voltage dependent, providing some uncertainties of interpretation. We aim to obtain parameters that can be assigned to a given situation, and measured by different techniques to show the coherence of the methods.

The procedure that achieves this goal is to use a "differential" or "small perturbation" method. Here the system is fixed at a steady state that is not affected by the perturbation associated to the measurement. Furthermore in this type of measurement one can apply a perturbation either in time, i.e. a step variation or a short square pulse, or in frequency domain, by a small oscillation perturbation with a certain angular frequency ω. A range of methods appears. The small perturbation techniques in the time domain are:[8]

- TPV, transient photovoltage, records the dynamics of the V_{oc} drop of a cell after it has been exposed to a short illumination pulse.
- TPC, transient photocurrent, records the dynamics of the current drop after a laser pulse.

And the small perturbation methods in the frequency domain are:[9]

- IS, impedance spectroscopy, gives the transfer function Z of a sinusoidal voltage with respect to a sinusoidal current.[10]
- IMPS, intensity-modulated photocurrent spectroscopy, gives the transfer function Q of a sinusoidal current with respect to a sinusoidal illumination flux.
- IMVS, intensity-modulated photovoltage spectroscopy, gives the transfer function W of a sinusoidal voltage with respect to a sinusoidal illumination flux.

In principle the time domain and frequency domain methods, if made over identical set of steady state conditions, must correspond to each other by the Laplace transformation. The correspondence is more or less complex depending on the properties of the system.[8] If a given device is fully controlled by recombination, the lifetime is not difficult to measure, as the time transient or frequency spectra can be interpretated unambiguously. But often, real devices are composed of different relaxation processes, associated to combination of transport, recombination, inhomogeneities, defect accumulations, interfaces, and so on. Then it is obtained multiple time constants or complex spectra, with more or less distinct features that need methods of interpretation to reach the recombination lifetime, separated from other ongoing processes.[11] The use of an equivalent circuit is substantial to the frequency techniques and provides an excellent framework to specify the models being used in each technique or approach and to achieve the separation of the existing dynamic components.[9]

There is, therefore, a significant opportunity to conciliate different methods to obtain a robust set of system parameters. In the studies of previous hybrid photovoltaic technologies it was established that analyzing the mechanisms of the lifetime requires to obtain high quality data over a wide variation of the splitting of the Fermi level.[12,13] Recombination in halide perovskites has been studied for many years, but recently some works have developed the correspondence of optical and electrooptical techniques over a wide voltage range.[14-16] In addition, progress has been obtained in the characterization of capacitances of halide perovskites.[9,17,18] Here we summarize the progress in this topic by formulating the conditions of observation of the lifetime in halide perovskites in terms of the capacitances in the system, and we show the correspondence of the models used in the time domain with the frequency domain methods. We also summarize the problems still existing for the measurement of the lifetime in order to point out further experimental determinations.

As explained before here we discuss the differential or small perturbation recombination lifetime τ_{rec}. The general concept has been explained in the textbook.[1] τ_{rec} is associated to a specific recombination mechanism as defined later in Eq. (7). There are other possible meanings of a lifetime: it can be a fit to a large signal or small signal observable (voltage, current, luminescence, conductivity, etc...). This will be denoted a "response time", associated to a given measurement.

The relation of the recombination lifetime to the response time[19] is a general problem that appears when applying the small perturbation methods mentioned above to measure

the lifetime. When the measurement is affected by additional factors related to electronic dynamics in the sample, such as capacitive charging, or trapping and detrapping effects, that occur prior to recombination, one obtains an "effective recombination time" τ_{eff} that is a response time. In many cases we have the decomposition

$$\tau_{eff} = \theta(V)\tau_{rec} \quad (1)$$

where θ is a factor that depends strongly on the difference of the Fermi levels of electrons and holes (expressed as a voltage V). Typically $\theta \gg 1$ indicating the additional time of the processes that slow down the measurement, composed with the fundamental electron-hole recombination events that take a time τ_{rec}.

In order to obtain the fundamental lifetime that can be observed by small perturbation techniques it is necessary to identify the non-recombinative effects that are included in $\theta(V)$. These effects have been well recognized in past technologies as the silicon solar cell (by the depletion capacitance)[10,14,20] organic solar cells (by capacitive charging)[21,22] and the dye-sensitized solar cell (by multiple trapping effects).[23,24]

For example, for the case of trap-limited recombination the factor is given by the variation of localized (n_L) to free carriers (n_c) in the conduction band:[24,25]

$$\theta(V) = \frac{\partial n_L}{\partial n_c} \quad (2)$$

The factor in Eq. (2) is valid in a quasistatic approximation, when trapping and detrapping is fast, for a small perturbation measurement.[23,26] This is because during measurement of the recombination lifetime you need to free a slice of localized charge when the Fermi level is displaced, as pointed out by Rose.[19] For an exponential tail of localized states Eq. (2) depends exponentially on voltage, so that exponential dependence of the lifetime observed in experiments may not be a property of the recombination mechanism.[27] In the multiple trapping model a similar effect exists for the diffusion coefficient,[28] and the correspondent factor is given by $(\partial n_L/\partial n_c)^{-1}$. It turns out that the measured diffusion length $L_{eff} = \left(D_{eff}\tau_{eff}\right)^{1/2}$ becomes independent of trapping factors.[23,24,26]

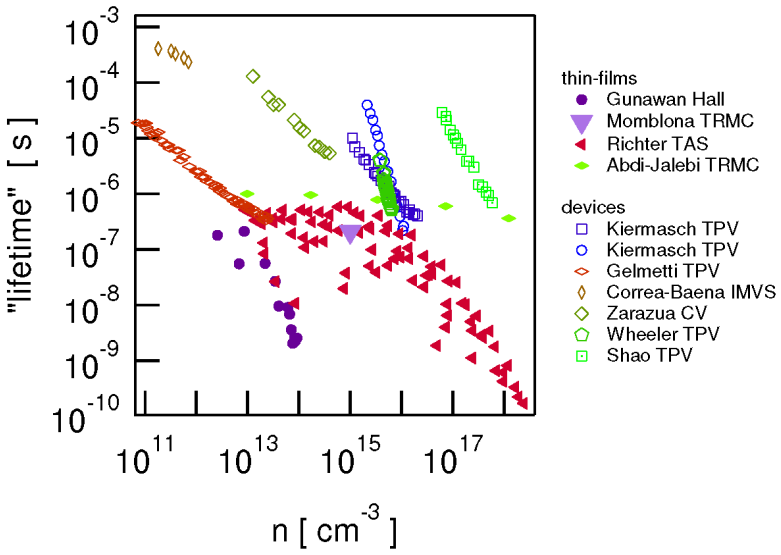

Fig. 1. Reported carrier lifetimes (derived from different techniques) versus carrier densities for thin-film (full) and devices (open symbols). Reproduced from Ref. [15]. Copyright: The Authors of Ref. [15].

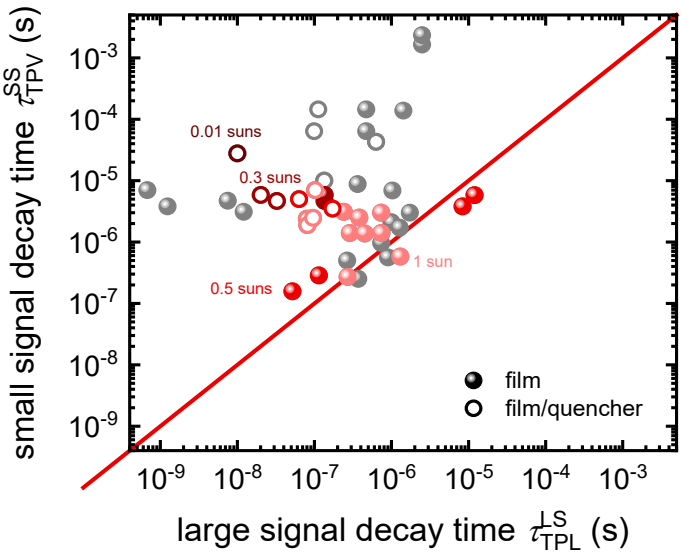

Fig. 2. Data collection from literature, comparing the decay time $\tau_{LS,TPL}$ of the transient PL measured on perovskite films (filled symbols) or on perovskite/transport layer stacks (blank symbols) with the stated decay time $\tau_{SS,TPV}$ resulting from transient photovoltage measurements on the respective solar cell device. The color code is linked to the bias light intensity during the TPV experiment ranging from light red (1 sun) to dark red (0.01 suns). For the grey data points, no information about the bias illumination level was available. The bisecting line (red) serves as a guide-to-the eye and indicates where both decay times are equal. The comparison of these decay times highlights that they correlate poorly and can differ by orders of magnitude. Interestingly, the decay time constant from the TPV

measurement is usually longer, although recombination losses are expected to be higher in the complete solar cell than in the pure perovskite film. Reproduced from Ref. [16]. Copyright: The Authors of Ref. [16].

A summary of the properties of the measured electron lifetimes in halide perovskites is presented in Fig. 1.[15] There are exponentially decreasing regions at increasing electron density, and also some regions of constant lifetime. Another important feature is shown in Fig. 2. The lifetime obtained by TPV is consistently larger than that measured by optical methods. It has been pointed out that some exponential dependencies and excess values are due to capacitive factors.[14-16,29] We now analyze the recombination model used in these references in order to obtain the excess factor of Eq. (1).

Let n the electron density. We assume that traps are saturated so that n represents free carriers. Their density depends on the voltage V as

$$n = n_0 e^{qV/m_0 k_B T} \tag{3}$$

Here q is the elementary charge, k_B is Boltzmann's constant, T the absolute temperature, and m_0 is an ideality factor. If electrons are minority carriers then $m_0 = 1$, while at high fluence $n = p$ we have $m_0 = 2$. For illustration of the methods we will assume this last value in the simulations, which is connected to measurement of lifetimes at high irradiation densities, although the actual values in high performance solar cells may be different.[30]

In a dynamic situation the variation of carrier density is

$$\frac{dn}{dt} = -U(n) + G - \frac{C_d}{qd}\frac{dV}{dt} \tag{4}$$

The recombination rate, U, and the generation rate, G, are both in cm^3 s^{-1}. Eq. (4) implies that the carrier density in steady state (indicated by overbar) is given by the solution of

$$U(\bar{n}) = \bar{G} \tag{5}$$

The first three terms in Eq. (4) are volumetric, and they are supposed to be the same throughout the film, so the system must be in homogeneous conditions such as the open-circuit. The last term of Eq. (4) accounts for capacitive charging of the electrodes separated a distance d, the thickness of the active film. The dielectric capacitance C_d is given in F cm^{-2}. The meaning of C_d is explained in more detail later. The factor $1/d$ converts the surface charge to volumetric charge.

We can prepare a homogeneous steady state and produce a small perturbation of the form $n = \bar{n} + \hat{n}(t)$, (with $\hat{n} \ll \bar{n}$), $V = \bar{V} + \hat{V}(t)$, etc. Consider the decay of a small perturbation of charge in the dark, for a sample without contacts. Eq. (4) gives

$$\frac{d\hat{n}}{dt} = -\frac{\partial U}{\partial n}\hat{n} \tag{6}$$

Whatever the form of $U(n)$, the decay is exponential, and the differential recombination lifetime is given by[24]

$$\tau_{rec} = \left(\frac{\partial U}{\partial n}\right)^{-1} \tag{7}$$

To make the meaning clear we adopt the recombination model that has been observed in many measurements of halide perovskites.[4,15,16,31-33]

$$U(n) = k_{rad} n^2 + \frac{n}{\tau_{SRH}} \tag{8}$$

Here k_{rad} is the coefficient for radiative band-to-band recombination, and τ_{SRH} is the lifetime for linear trap-assisted Shockley-Read-Hall recombination. Inclusion of Auger recombination is not normally necessary in the framework of the methods commented here. From Eq. (7) we obtain the total recombination lifetime as the sum of the two parallel pathways

$$\tau_{rec} = \left(\frac{1}{\tau_b} + \frac{1}{\tau_{SRH}}\right)^{-1} \tag{9}$$

where

$$\tau_b = \frac{1}{2\, k_{rad}\, \bar{n}} \tag{10}$$

If we apply a small perturbation of voltage or incident light, the systems responds according to the equation obtained from Eq. (4)

$$\left(\frac{\partial n}{\partial V} + \frac{C_d}{qd}\right)\frac{d\hat{V}}{dt} = -\frac{\partial U}{\partial n}\frac{\partial n}{\partial V}\hat{V} + \hat{G}$$

$$\left(qd\frac{\partial n}{\partial V} + C_d\right)\frac{d\hat{V}}{dt} = -\frac{1}{\tau_{rec}} qd\frac{\partial n}{\partial V}\hat{V} + qd\hat{G} \tag{11}$$

Let us introduce some convenient quantities. The chemical capacitance is[34]

$$C_\mu = qd\frac{\partial n}{\partial V} \tag{12}$$

The factor d makes C_μ expressed in F cm^{-2}. The generation flux Φ_g (in cm^{-2}) is

$$\Phi_{\mathrm{g}} = -d\, G = \varphi_g \Phi_{\mathrm{in}} \tag{13}$$

where φ_g is a generation efficiency and Φ_{in} is the incoming light flux per unit area (cm^{-2}). Eq. (11) can be presented as

$$\left(C_\mu + C_d\right)\frac{d\hat{V}}{dt} = -\frac{1}{\tau_{rec}} C_\mu \hat{V} - q\varphi_g \hat{\Phi}_{in} \tag{14}$$

Suppose that $\hat{\Phi}_{in} = 0$ during the measurement. Then from Eq. (14)

$$\tau_{eff} = \left(1 + \frac{C_d}{C_\mu}\right)\tau_{rec} \tag{15}$$

We reach the conclusion that the lifetime is *directly* measured only if the chemical capacitance is larger than the dielectric capacitance. In the domain in which $C_d > C_\mu$, the dominant process is a discharge of the dielectric capacitance. The effective lifetime is larger than the recombination lifetime, as indicated in the observations of Fig. 2, by the factor $\theta(V) = C_d/C_\mu$.

In the model of Eq. (14) we have generally termed "dielectric capacitance" any capacitance that responds to the electrical field, either in very short range, as the surface ionic polarization, or in long range, as the bulk dielectric response. In an optoelectronic

semiconductor device C_d can have different origins:[18] (a) The metal contacts contribute a constant capacitance, affected by additional specific capacitances due to compact or passivating layers,[35] and in the presence of mobile ions the contacts include a Helmholtz capacitance. (b) A semiconductor depletion capacitance is voltage-dependent as characterized in Mott-Schottky plots. (c) The bulk dielectric response (the geometric capacitance), can also be considered constant as a function of voltage. All these terms are included into the dielectric capacitance C_d in a broad sense.

On the other hand the chemical capacitance is due to the increase of the chemical potential and does not consider electrical field dependence. This distinction is expressed in the textbook.[1] According to (12) C_μ increases exponentially with the photovoltage as

$$C_\mu = \frac{q^2 d n_0}{m_0 k_B T}\, e^{qV/m_0 k_B T} \tag{16}$$

The chemical capacitance can be measured directly in silicon[20,36,37] and organic devices.[38-40] It has the same ideality factor m_0 as that of the carrier density (3).

Consider Eq. (14) in the dark and with negligible recombination. Then a voltage transient produces the result $C_\mu = -C_d$ that seems a charge compensation equation to satisfy electroneutrality. But in the simple model of Eq. (14) the chemical capacitance and dielectric capacitance are not connected by charge neutrality.[1] In order to obtain strict charge compensation one needs to establish a complete semiconductor model of the device (involving Poisson equation, etc.).[41] The model of Eq. (14) must be taken as a first approximation to the capacitive response that only indicates which type of capacitance is dominant for the measurement of the dynamic properties.

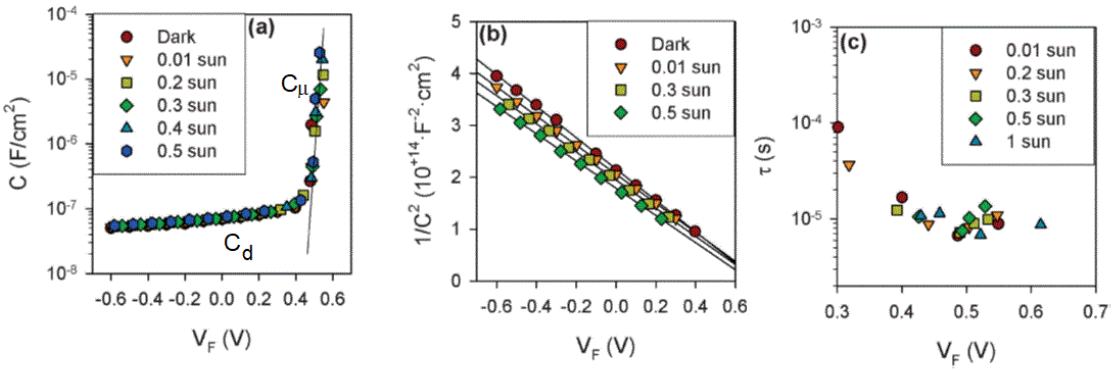

Fig. 3. Electrical response of a monocrystalline silicon solar cell. (a) Device capacitance as a function of Fermi-level potential, V_F, for different light intensities. Solid line represents the fit of C in the potential region where the chemical capacitance C_μ is dominant. The depletion capacitance C_d that is the dominant contribution to the cell capacitance at low voltage is represented separately in (b) as a Mott–Schottky plot. (c) Minority carrier lifetime as a function of Fermi level potential obtained as the product of the recombination resistance and total capacitance. Reproduced from Ref. [10]. Copyright: The Royal Society of Chemistry, 2009.

Fig. 4. Calculated effective differential lifetime for a Si photodiode together with measured ones from OCVD and TPV. The capacitance value used is to 2×10^{-4} F m^{-2} . Reproduced with permission from [14]. Copyright: The Royal Society of Chemistry, 2019.

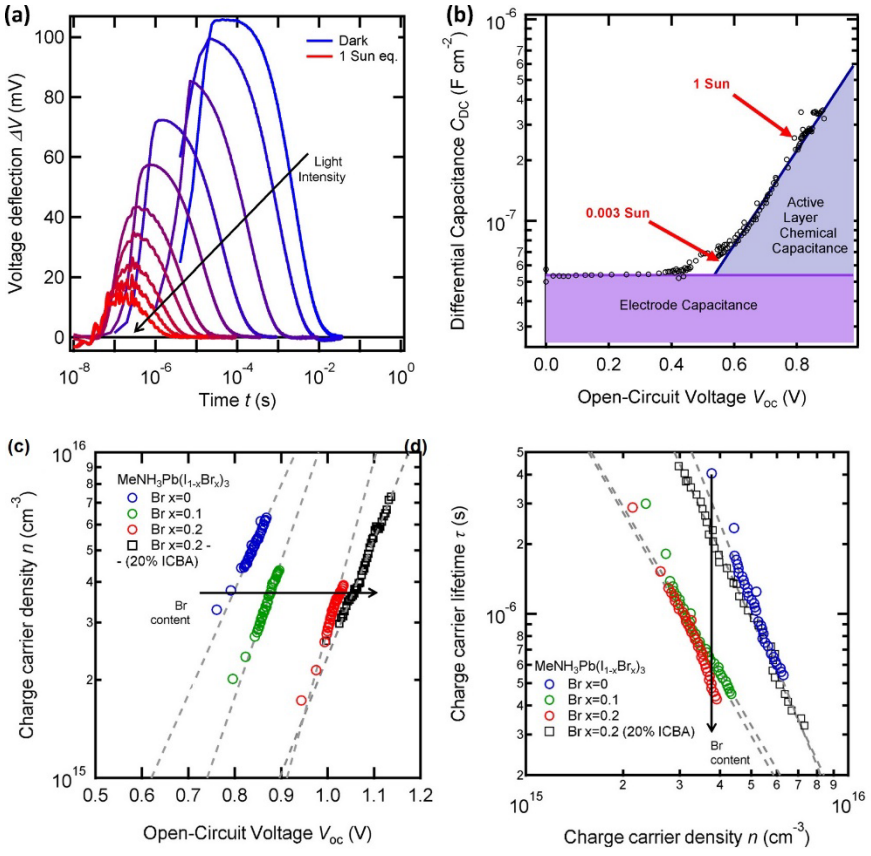

Fig. 5. Transient voltage and capacitance response of halide perovskite solar cells: (a) Decay of the transient photovoltage over a range of light intensities between darkness and 1 sun for a $CH_3NH_3PbI_3$ planar hybrid perovskite. (b) Differential capacitance measured from transient photocurrent and transient photovoltage as a function of the open-circuit voltage (V_{oc}) over a range of background light intensities from 0 to 5 sun equivalents. (c) Active-layer charge-carrier density (n) as a function of quasi-Fermi-level splitting (V_{oc}). (d) Average charge-carrier lifetime (τ) as a function of n for $CH_3NH_3Pb(I_{1-x}\,Br_x)_3$ cells with Br contents of x = 0, 0.1, and 0.2. The same approximate range of light intensities, between 0.1 and 3 sun equivalents, was used for each material system. The results for the use of 20% ICBA in PCBM for the x = 0.2 device is shown with black squares. Reproduced from Ref. [42]. Copyright (2017) American Chemical Society.

Let us review some results of the literature that consider Eq. (15). Fig. 3 shows a silicon solar cell measured by Mora-Seró et al.[10] In Fig. 3a and b it is clearly observed that the dominant capacitances in the cell are a depletion capacitance at low voltage and the chemical capacitance at high voltage. The transition occurs approximately at 0.4 V. Above this value the lifetime is a constant, Fig. 3c, but below 0.4 V the RC product is affected by the large dielectric capacitance and the result is not a recombination lifetime.

Kiermasch et al.[14] also showed the lifetime for a silicon device, Fig. 4. For a constant dielectric capacitance we have

$$\tau_{eff} = \left(1 + \frac{C_d m_0 k_B T}{q^2 d n_0}\, e^{-qV/m_0 k_B T}\right) \tau_{rec} \tag{17}$$

Thus the effective lifetime decreases exponentially until the chemical capacitance becomes large enough and reveals the constant recombination lifetime.

Finally Wheeler et al.[42] present in Fig. 5a and b the results of differential charging. The chemical capacitance predominates clearly over the substrate capacitance at 0.6 V. As a result the carrier density can be measured above 0.6 V and the correspondent TPV time constant in Fig. 5d gives directly the recombination time.

We now consider the application of the effective and recombination lifetime to the measurement of halide perovskite solar cells. By Eqs. (9) and (17) we obtain

$$\tau_{eff} = \left(1 + \frac{C_d}{C_\mu}\right)\left(\frac{1}{\tau_b} + \frac{1}{\tau_{SRH}}\right)^{-1} \tag{18}$$

Normally the radiative lifetime τ_b that decreases at increasing voltage, becomes dominant (smaller) at high fluence or carrier density. With respect to Eq. (17) we use a more general form of the dielectric capacitance since it is often observed to depend exponentially on the voltage, as shown in Fig. 6.[9] This topic will be further discussed later, and we assume

$$C_d = C_{d0} + C_{d1}\, e^{qV/m_1 k_B T} \tag{19}$$

C_{d0} and C_{d1} are constants and m_1 is the ideality factor of the capacitance. C_{d0} is a capacitance related to surface polarization. In the simulations, distances are in cm, time

in s, voltages in V, charge in C, capacitance in F. For a general illustration of Eqs. (18-19), Fig. 7a shows the interplay of capacitances and Fig. 7c shows the effective (red) and true (blue) recombination lifetime as well as their different components. We note the transition of recombination mechanisms in the blue line, but both are distorted in τ_{eff} by the capacitive factor, until when $C_\mu > C_d$, that they match each other $\tau_{rec} = \tau_{eff}$ as explained earlier. By Eq. (3) the carrier density is exponential with the voltage, Fig. 5c and Fig. 7b, so that one can represent the lifetimes either *vs.* voltage or carrier density, without changing the form.

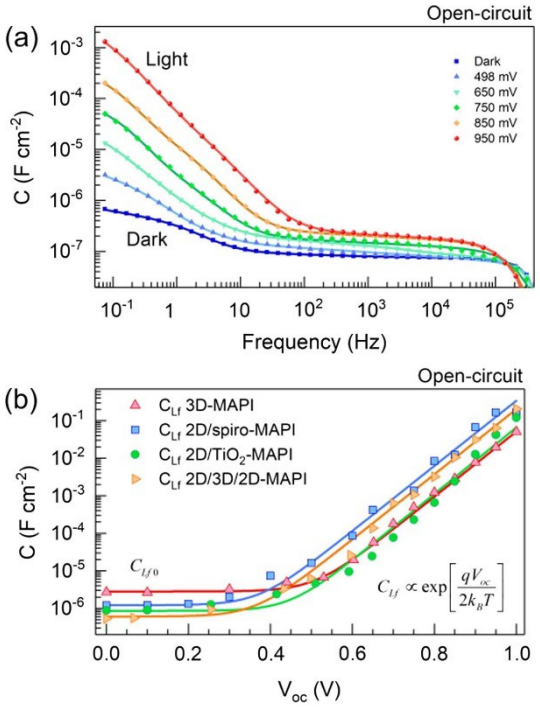

Fig. 6. (a) Capacitance spectra as a function of for a $CH_3NH_3PbI_3$-based perovskite solar cell. (b) Low-Frequency capacitance for several devices based on $CH_3NH_3PbI_3$ and a variety of interlayers (2D perovskite thin capping) also as a function of V_{oc}. Reproduced from Ref. [43]. Copyright (2019) Elsevier.

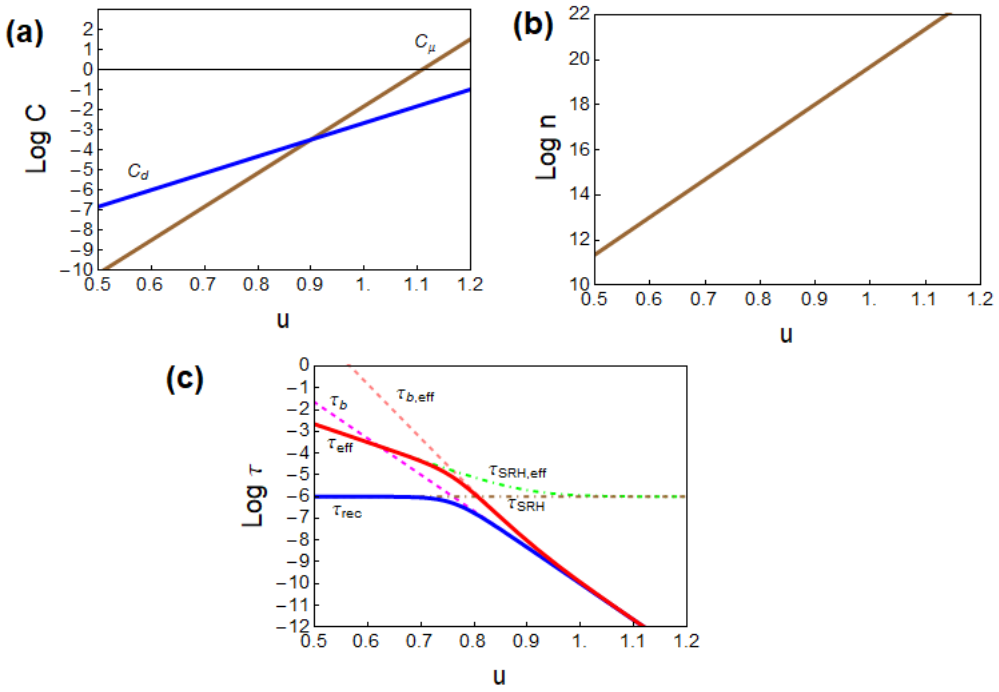

Fig. 7. Simulations of (a) dielectric and chemical capacitances, (b) carrier density and (c) lifetimes as a function of voltage (separation of Fermi levels). u is the voltage excluding the drop in the series resistance. Shown in (c) are the recombination lifetime τ_{rec} (blue), the measured lifetime τ_{eff} (red) and their different components in dashed and dot-dashed lines. Parameters $\mathrm{C_{d0}} = 0$; $\mathrm{C_{d1}} = 10^{-11}$ F cm^{-2}; $\mathrm{m_0} = 1; m_1 = 2$; $\mathrm{k_{rec}} = 1.0 \times 10^{-10}$ cm^3 s^{-1}; $\tau_{\mathrm{SRH}} = 1.0 \times 10^{-6}$ s; $d = 500 \times 10^{-7}$ cm; $q = 1.6 \times 10^{-19}$ C; $\mathrm{n_i} = 1 \times 10^3$ cm^{-3}; $\mathrm{k_B\,T} = 0.026$ eV.

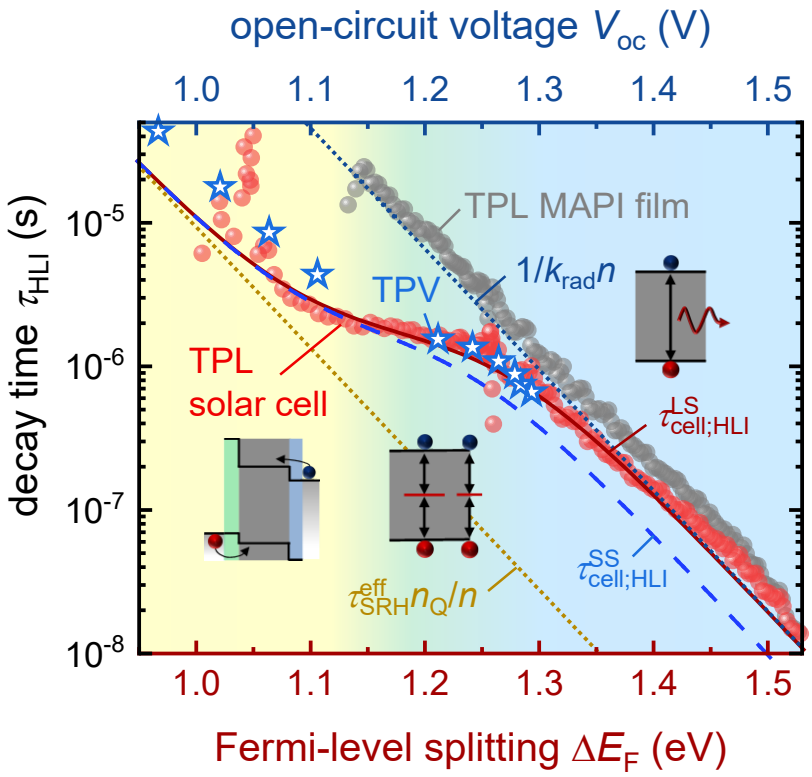

Fig. 8. Experimental data of the decay time derived from large-signal TPL measurements ($\tau_{LS,TPL;HLI}$) of a perovskite film (grey spheres) and the solar cell (red spheres) and TPV measurements ($\tau_{SS,TPV;HLI}$) at different bias illumination intensities (blue stars). Furthermore, the exponential slope of the capacitance-dominated (light yellow) and the radiatively dominated (light blue) regions are shown as guide to the eye. An analytical model is indicated for small- (blue dashed line) and large-signal (red solid line) transients on cells. Reproduced from Ref. [16]. Copyright: The Authors of Ref. [16].

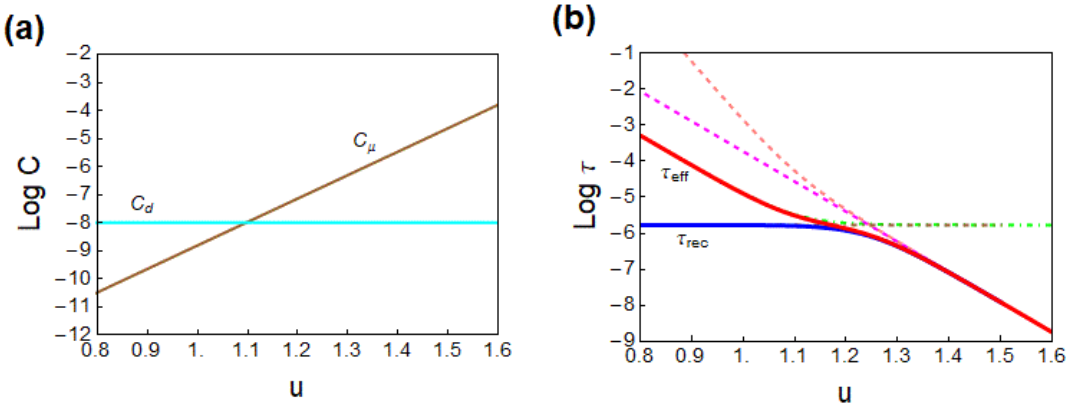

Fig. 9. Simulations of (a) dielectric and chemical capacitances and (b) lifetimes. u is

the voltage excluding the drop in the series resistance. Shown are the recombination lifetime τ_{rec} (blue), the measured lifetime τ_{eff} (red) and their different components in dashed and dot-dashed lines. Parameters taken from Ref. [16]: $C_d = 10^{-8}$ F cm^{-2}; $m_0 = 2$; $k_{rec} = 1.5 \times 10^{-10}$ cm^3 s^{-1}; $\tau_{SRH} = 1.7 \times 10^{-6}$ s; $d = 280 \times 10^{-7}$ cm; $q = 1.6 \times 10^{-19}$ C; $n_i = 8 \times 10^4$ cm^{-3}; $k_B T = 0.026$ eV.

Fig. 10. (a) Determination of lifetimes by combined TAS (red) and time-delayed-collection-field (TDCF) (blue) under 0.1 sun equivalent background illumination on full devices at V_{oc}. B) Differential lifetimes deduced from Transient charge carrier dynamics under 0.1 sun equivalent background illumination and TAS (triangles) and from TPV (red circles) as a function of carrier density. The red line shows the limit for TPV measurements according to Kiermasch et al.,[14] the solid line shows the numerical derivative of the total fit (purple) and the dashed lines the corresponding contributions as denoted. Reproduced from Ref. [15]. Copyright: The Authors of Ref. [15].

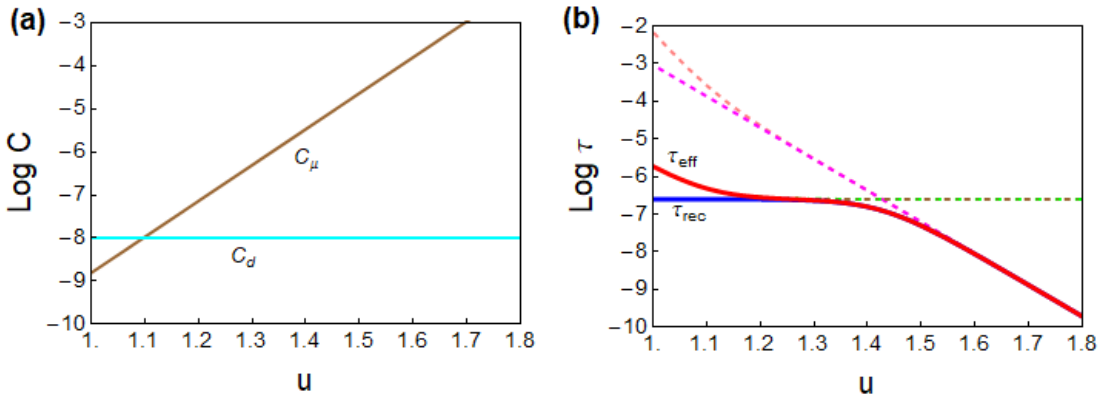

Fig. 11. Simulations of (a) dielectric and chemical capacitances and (b) lifetimes. u is the voltage excluding the drop in the series resistance. Shown are the recombination lifetime τ_{rec} (blue), the measured lifetime τ_{eff} (red) and their different components in dashed and dot-dashed lines. Parameters taken from Ref. [15]: $\mathrm{C_d} = 10^{-8}$ F cm^{-2}; $\mathrm{m_0} = 2$; $\mathrm{k_{rec}} = 3 \times 10^{-11}$ cm^3 s^{-1}; $\tau_{\mathrm{SRH}} = 0.25 \times 10^{-6}$ s; $d = 280 \times 10^{-7}$ cm; $q = 1.6 \times 10^{-19}$ C; $\mathrm{n_i} = 8 \times 10^4$ cm^{-3}; $\mathrm{k_B\,T} = 0.026$ eV.

Based on the general model (18) we discuss specific results about halide perovskites given in the literature. The data in Fig. 8 by Krückemeier et al.[16] are highly significant as it compares the film with and without contacts, to identify the effect of the electrodes over a wide range of voltages. They show large-signal TPL measurements of a perovskite film (grey spheres) and the solar cell (red spheres), and TPV measurements (stars). The downward displacement of the TPV data that includes non-radiative recombination, with respect to the grey data of the contactless samples, is due to the combination of two electrode effects: appearance of significant linear recombination, and the capacitive effect, as outlined for the same parameters in Fig. 9a and b, in which a constant C_d is adopted.

Fig. 10 obtained by measurements of TAS by Wolff et al. shows the constant lifetime region at low voltage, modified by a small constant capacitive factor, and the transition to the radiative lifetime τ_b. The different quantities inferred from the experimental parameters are summarized in Fig. 11. In Fig. 10 the region of constant lifetime is better appreciated than in Fig. 8. This is because Fig. 10 has a shorter τ_{SRH}. The parameter $\mathrm{n_i}$ is very important as it fixes the value of the chemical capacitance. It is taken the same value in both simulations.

Incidentally we remark that the large signal measurement and small perturbation methods can be put easily into correspondence if (1) the lifetime is measured separately in the given method, and (2) the functional form is a constant or an exponential dependence with voltage,[6] see Fig. 4 and 8. In the case of multiple relaxation phenomena, a more involved method of integration from a set of small perturbation measurements can be used to obtain the response to a large voltage sweep, as in the case of hysteresis in current-voltage curves.[44] Alternative full drift diffusion numerical simulations can address different methods.[45]

The previous reasoning is based on the time domain decay techniques represented by Eq. (14). Now we want to develop the electrical analogues of the model in order to apply it to the small perturbation frequency techniques. The recombination resistance is defined as[24]

$$R_{rec} = \left(qd\frac{\partial U}{\partial V}\right)^{-1} \tag{20}$$

We can express Eq. (14) as

$$\left(C_\mu + C_d\right)\frac{d\widehat{V}}{dt} + \frac{1}{R_{rec}}\widehat{V} + q\widehat{\Phi}_g = 0 \tag{21}$$

Clearly this last result consists on the addition of three small perturbation currents:

capacitive, recombination, and photogeneration, respectively. Furthermore Eq. (21) is for the techniques operating at open circuit, that is an assumption of Eq. (4). If we allow electrical current extraction I through the contacts we can write more generally

$$\hat{I} = \left(C_\mu + C_d\right)\frac{d\hat{V}}{dt} + \frac{1}{R_{rec}}\hat{V} + q\hat{\Phi}_g \tag{22}$$

The correspondent generalization of the large signal equation (4) is

$$I = qd\frac{dn}{dt} + C_d\frac{dV}{dt} + qd\,U + q\Phi_g \tag{23}$$

For the small perturbation measurements at the angular frequency ω we use the Laplace transformation $d/dt \rightarrow i\omega$. Eq. (22) gives

$$\hat{I} = \left[\left(C_\mu + C_d\right)i\omega + \frac{1}{R_{rec}}\right]\hat{V} + q\hat{\Phi}_g \tag{24}$$

This last equation can be translated into the equivalent circuit of Fig. 12a. $\hat{I}$ is the current across the series resistance R_s, and the voltage between the external connections is

$$\hat{V}_{ext} = R_s\hat{I} + \hat{V} \tag{25}$$

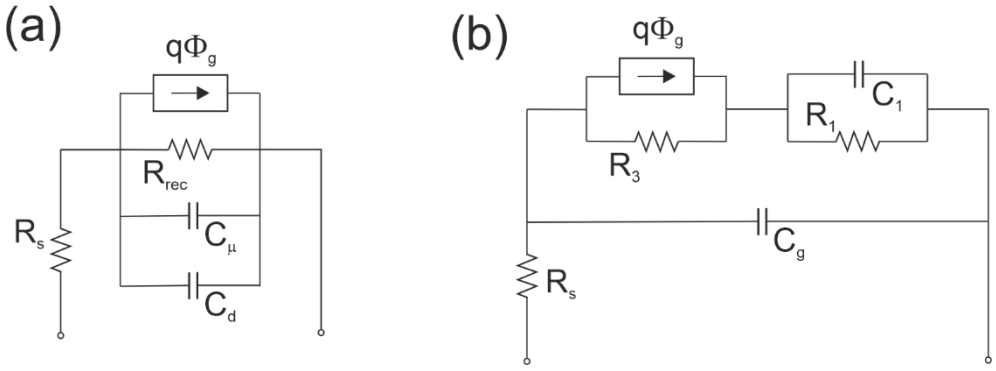

Fig. 12. Equivalent circuit representation of small perturbation models. $q\hat{\Phi}_g$ is a current generator that stands for photogeneration current. (a) Simple recombination model of Eq. (21) with added series resistance R_s. (b) Standard circuit for halide perovskites frequency techniques.

The circuit in Fig. 12a provides a useful picture for the interpretation of the excess apparent lifetime. By Eq. (7), (12) and (18) we obtain the identity

$$\tau_{rec} = R_{rec}C_\mu \tag{26}$$

In the equivalent circuit approach the recombination lifetime is a time constant of the type $\tau = RC$. From the impedance spectra, one can obtain the different resistances and capacitor elements, and many types of capacitors are possible in complex devices.[35] In the model of Fig. 12a, the dominant capacitance will prevail. Only if $C_\mu > C_d$ the product $\tau = RC$ is interpreted as a recombination lifetime, as indicated in Eq. (26). Therefore a main criterion to obtain a recombination lifetime in homogeneous conditions is the clear observation of the chemical capacitance, as indicated in Fig. 5b.

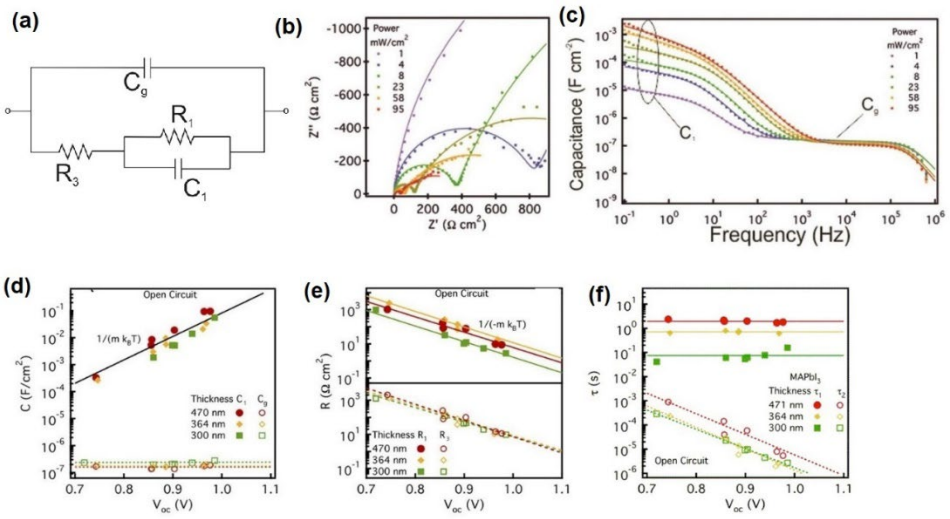

Fig. 13. Impedance spectroscopy results of a planar structure FTO/TiO_2/$MAPbI_3$/spiro-OMeTAD/Au solar cell. (a) Equivalent circuit model. (b) Example of complex plane impedance plot measured under short-circuit conditions at different irradiation intensities. Solid lines correspond to fits using the EC of (a). (c) Example of capacitance spectra corresponding to the conditions in panel (b). (d) Capacitances, (e) resistances and (f) characteristic times under open-circuit conditions. Solid lines (low-frequency arc) and dashed lines (high-frequency arc) correspond to linear fits with m approaching 2, in agreement with a second order recombination. In panel d, $m = 1.90 \pm 0.17$, and in panel e, $m = 1.94 \pm 0.08$. Reproduced from [46]. Copyright (2016) American Chemical Society.

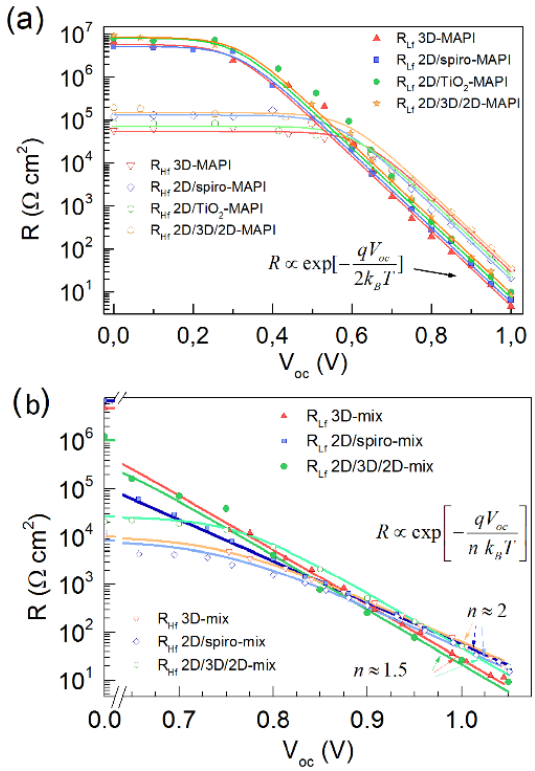

Fig. 14. High- and low-frequency resistance as a function of voltage for a variety of solar cells containing different perovskite absorbers 3D layers based on (a) $CH_3NH_3PbI_3$ or (b) mixed $Cs_{0.1}FA_{0.74}MA_{0.13}PbI_{2.48}Br_{0.39}$ and a variety of interlayers (2D perovskite thin capping). Adapted with permission from [43]. Copyright (2018) Elsevier.

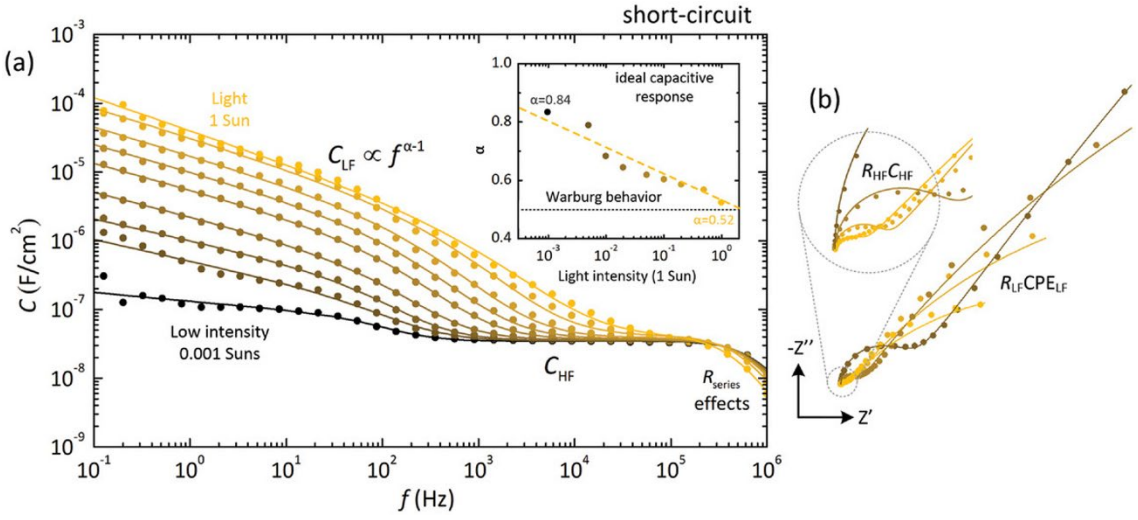

Fig. 15. a) Capacitance spectra and b) impedance plots, measured under short-circuit conditions (0 V) between 1 MHz and 100 mHz, for 600 nm thick CsFAPbIBr-based solar cells as a function of illumination intensity. Inset of (a): CPE low frequency exponents from the non-ideal low-frequency relaxation processes, α, versus light intensity. Permission [47].

In the field of metal halide perovskites a multitude of measurements of IS and also studies of IMVS and IMPS have been presented, and the knowledge has been summarized recently.[9,48] An equivalent circuit usually used in these measurements is outlined generally in Fig. 12b for any small perturbation measurement, and it reduces to that of Fig. 13a for the case of impedance spectroscopy. The circuit shows two arcs in the impedance complex plane, Fig. 13b, and two correspondent capacitances. C_1 is a low frequency capacitance that increases strongly with illumination, while C_g is a nearly constant high frequency dielectric (geometric) capacitance,[49] as indicated in Fig. 6a and in Fig. 13d. Very often a third arc associated to contact layers with an additional capacitance contribution can be observed.[50,51]

In the simplest impedance response of Fig. 13a, two resistances are observed that dominate the high frequency (R_3) and low frequency (R_1) ranges, respectively. The properties of these resistances are shown in Fig. 14. Note in Fig. 14 that the shunt resistance dominates at low voltages. In some cases these resistances display a similar dependence on illumination and voltage.[46,52] This is particularly observed for 3D perovskite in the simplest formulations as shown in Fig. 14a for $MAPbI_3$-based planar solar cells with four different contacting layers. Both resistances exhibit voltage-dependences of the type $R \propto e^{-qV/2k_BT}$ at high forward potentials. These resistances are interpreted as components of the recombination resistance, Eq. (20), indicating that similar densities of electrons and holes participate in a second order carrier recombination mechanism, in agreement with the curves in Fig. 8 and 10b at large V_{oc} values. However, for multicomponent perovskite absorbing layers shown in Fig. 14b the two resistances behave differently, with exponents $m = 2$ and $m = 1.5$, indicating a much more complex situation associated to decoupling of recombination mechanisms.[43]

The circuit of Fig. 12b is not unique. There are other possible connections used by different authors. This question has been reviewed recently.[9,53] However, the main point to illustrate here is that the circuit 12a that arises from the recombination model (4) has two capacitances in parallel and gives only one arc in the impedance complex plane. While the impedance data requires two distinct capacitors that are visible by the presence of different internal resistances. The capacitances are clearly distinguished in the representation as a function of frequency, Fig. 6a and Fig. 13c. The constant C_g is neatly separated at high frequencies. However, the issue becomes more complicated since the rise of the capacitance can occur at very high frequency, as shown in Fig. 15.

There is a large disparity of the results of IS shown in Fig. 13 and 14 and those about measured lifetimes shown previously in Fig. 5, 8 and 10. The main problem is that IS does not resolve the chemical capacitance, probably because $C_\mu \ll C_d$. It has been shown that in contrast to Si devices, chemical capacitances in halide perovskites are not easily observed,[17] mainly due to a low DOS value.[18] In fact Mora-Seró and coworkers documented the vanishing of the chemical capacitance when increasing the amount of

perovskite in the solar cell.[53] This property relates to the contrast of lifetime and relaxation semiconductors.[54] On the other hand the observed resistances dependence on voltage are compatible with recombination mechanisms obtained in the transient methods.

Let us observe this question in more detail. In Fig. 13f we obtain two separate time constants. Firstly $\tau_1 = R_1 C_1$ is a constant at all voltages due to the exponential increase of C_1 shown in Fig. 13d. But τ_1 is in the range of s and cannot correspond to a recombination lifetime. It has been interpreted in terms of a combination of ionic-electronic phenomena.[55] On the other hand $\tau_3 = R_3 C_g$ shows an exponential decrease in agreement with Fig. 5, 8 and 10 but the values of τ_3 from IS are much higher than those of the other methods. Furthermore the high frequency capacitance of Fig. 13c does not show the chemical capacitance, in contrast to Fig. 5 and 10. Therefore τ_3 cannot be interpreted as a recombination lifetime. Nevertheless some authors have proposed a correspondence of the different techniques. One example is discussed later.

In summary there is a general problem for the interpretation of the time constants of IS as a recombination lifetime, since there is not a clear correspondence between the model that describes well the IS results, Fig. 12b, and that used for the analysis of lifetimes, Fig. 12a. This introduces a major problem for the interpretation of how lifetime measurements are affected by capacitive contributions in the C_d component in Eq. (18). We have indicated a general dependence in Eq. (19), because as already mentioned the capacitance contains several components. One can see in Fig. 6a, 13c and 15 that the variable component of the capacitance reaches the high frequencies and can affect the lifetimes measured by time transient methods. Therefore, regarding the observed properties of capacitance as directly measured by IS, the chemical capacitance is not observed and in addition it is not straightforward to determine which dielectric capacitance value should be applied in a given decay experiment to correct the distortion of the lifetime. To solve this problem, it seems necessary to provide an equivalent circuit consistent with both, time decays and the transfer functions of frequency methods, at the same time. A correlation of different methods that was realized for organic[22] and silicon[56] solar cells has not been established so far for halide perovskites.

In support of the required correlation of methods that we just mentioned, we recall that by using frequency-modulated illumination as an additional input, two additional methods are obtained that may be correlated to IS: the IMVS and IMPS. In fact IMVS applied at open circuit is a method used to determine electron lifetimes[57,58] and the quality of the solar cells.[59] There have been presented abundant studies of IMPS in halide perovskites.[60-63]

For an equivalent circuit that represents a system as in Eq. (23) and Fig. 12a, operated by three external stimuli (V, I, Φ), there are three possible separate output/input transfer functions, by elimination of one variable in each case in Eq. (23), as indicated in Table 1.[8,64] The corresponding modes of measurement are shown in Fig. 16. An example of the results[51] of the three methods is shown in Fig. 17 for carbon-based perovskite solar cells that consist of a scaffold of mesoporous TiO_2 and ZrO_2 layers infiltrated with perovskite

and do not require a hole-conducting layer.[65] Note the negative feature in the real axis of IMPS that will be further discussed in the following. It must be also remarked the different convolutions occurring at low frequency that can be ascribed to ionic-electronic phenomena including chemical inductors.[66-68]

Table 1. Transfer function of small perturbation frequency techniques.

Method	$\hat{I}$	$\hat{V}$	$q\widehat{\Phi}_{in}$	Transfer function
IS			0	$Z = \hat{V}/\hat{I}$
IMPS		0		$Q = \hat{I}/q\widehat{\Phi}_{in}$
IMVS	0			$W = -\hat{V}/q\widehat{\Phi}_{in}$

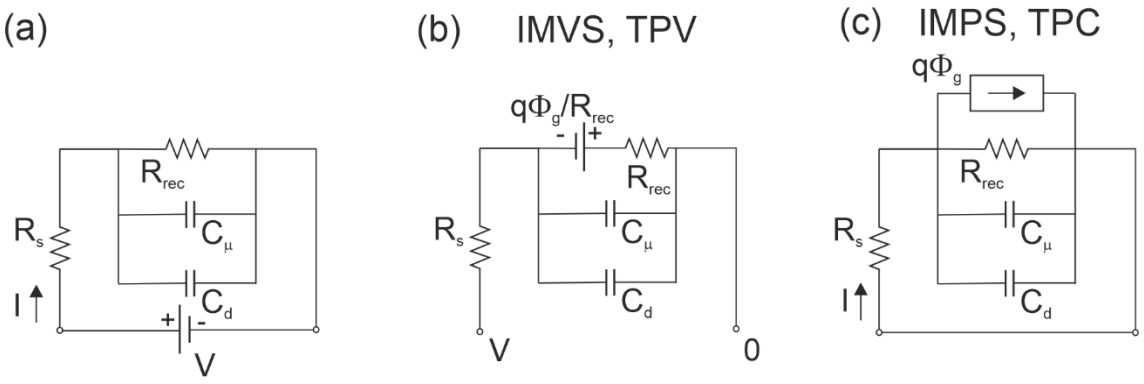

Fig. 16. Different setups for the measurement of transfer functions of the model of Fig. 11a.

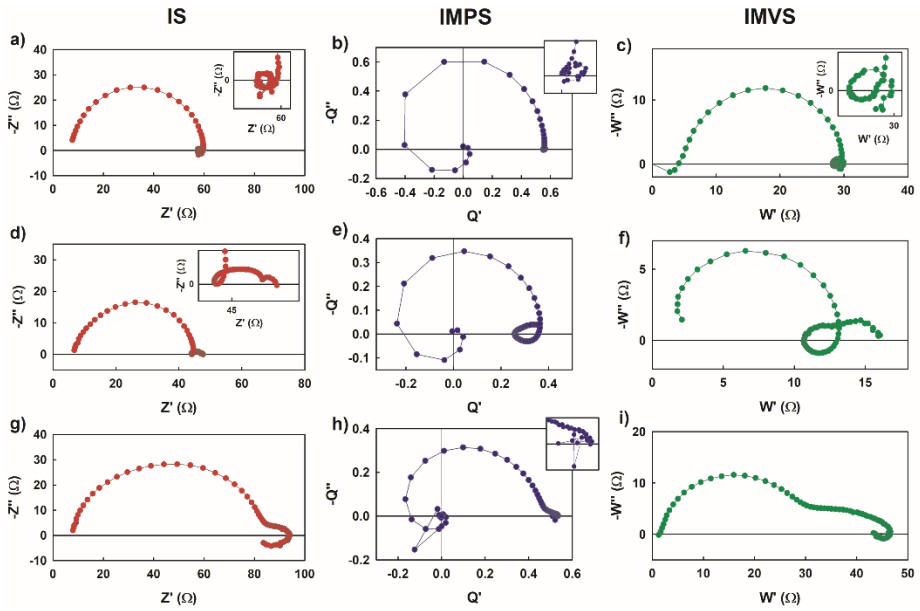

Fig. 17. Complex plane plots of the IS (red), IMPS (blue) and IMVS (green) transfer

functions (Z, Q and W, respectively) for a carbon halide perovskite device measured under 0.1 sun illumination, for a frequency range of 1 MHz to 0.01 Hz and at open circuit voltage. The three rows from top to bottom correspond to cells with regular, double, and triple thicknesses. Adapted with permission from [51]. Copyright (2020) American Chemical Society.

The identification of the equivalent circuit and its interpretation using independent measurements at the same condition is a major resource for a robust interpretation of the dynamical features of a device.[52,61] In the case of Fig. 16 the spectral shapes should be quite simple. But in practice the situation is complicated by multiple processes, as indicated earlier. It has been shown that an analysis by IMPS reveals distinct features that are lumped in IS.[60]

Consider a general physical model that allows the three independent variations of a device, as in the example of Eq. (24). As shown by Bertolucci et al. [64], we obtain a relationship of the type

$$\hat{I} = S(\bar{V}, q\bar{\Phi}_{in})\hat{V} + T(\bar{V}, q\bar{\Phi}_{in})q\hat{\Phi}_{in} \tag{27}$$

From the Table 1 we can see that Eq. (27) takes the form

$$\hat{I} = \frac{1}{Z}\hat{V} + Qq\hat{\Phi}_{in} \tag{28}$$

Therefore, when we arrive at an equation of the type (27), then we have found the transfer functions since $Z = S^{-1}$ and $Q = T$. As the three transfer functions in Table 1 arise from the small perturbation of a general model function, the triple product rule of the partial derivatives imposes a restriction over the possible values.[8] The constraint between the three transfer functions is

$$W = QZ \tag{29}$$

The relation (29) has been exploited in recent publications.[51,69] Ref. [8] has provided the connection between the time and frequency domain for a range of models, including that in Fig. 16. Fig. 18 shows the correlation between the time constants of IS, TPV and IMVS of two different halide perovskites solar cells.[29] The match is excellent in both cases. However, the question if this time constant can be interpreted as a recombination lifetime, depends on the observation of the chemical capacitance, as commented earlier.

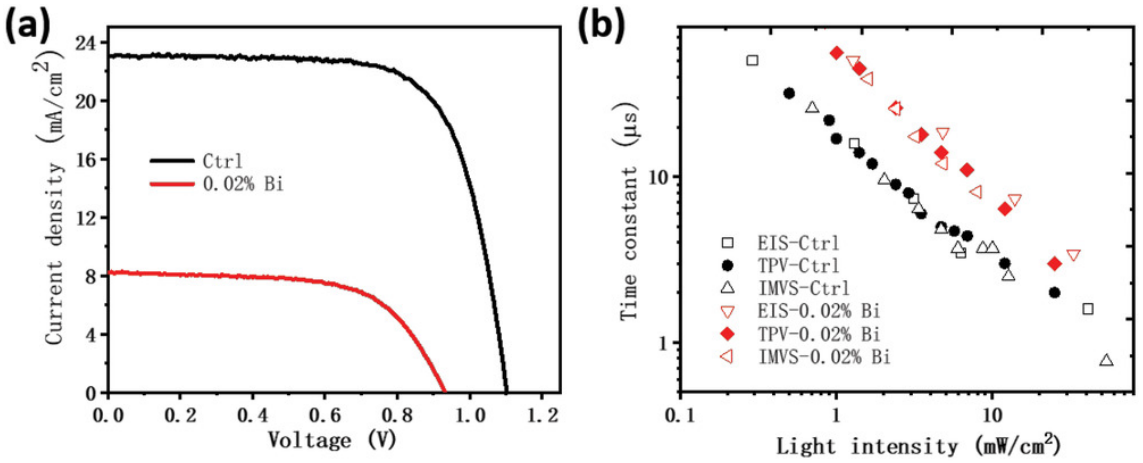

Fig. 18. Characterization of solar cells with low (Ctrl) and high defect concentrations (0.02% Bi). a) JV curves of devices measured under simulated solar light (scan rate of –50 mV s^{-1}). b) Small signal perturbation data from TPV, IMVS, and IS measured under white LED light. Reproduced from Ref. [29]. Copyright: The authors of Ref. [29].

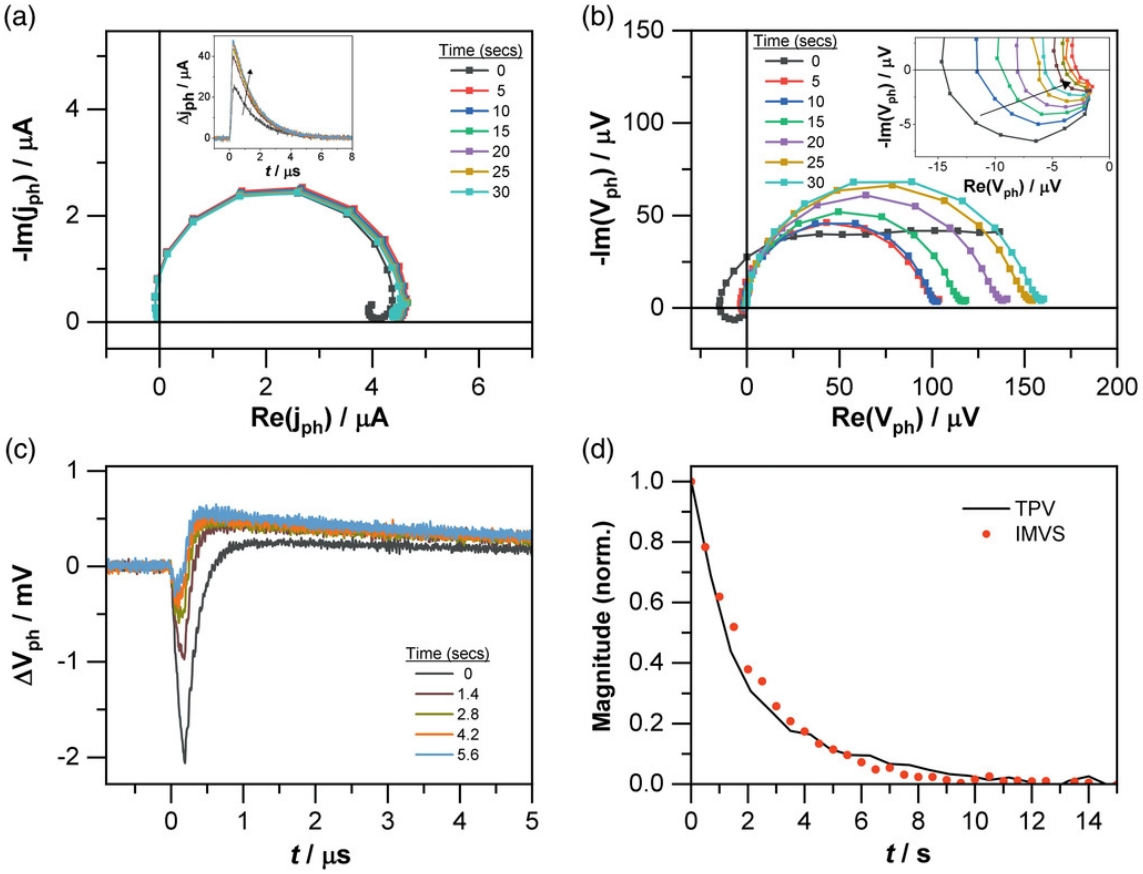

Fig. 19. a) Progression of IMPS response for SnO_2 based perovskite solar cell at 5 s intervals, showing that no negative photocurrent signal is observed (inset: TPC progression for same SnO_2 device at 1.4 s intervals, showing that no negative TPC signal

is seen even at short times after illumination). b) Progression of IMVS response for SnO_2 cell at 5 s intervals (inset: 0.5 s intervals for first 5 s after illumination). c) TPV response at 1.4 s intervals. d) Comparison of the relative magnitude of the negative photovoltage signal from IMVS and TPV measurements of SnO_2 device. Reproduced from Ref. [70]. Copyright: The authors of Ref. [70].

The work on Fig. 19 by Pockett et al.[70] shows and excellent correlation of nontrivial features in time and frequency domain. The IMVS shown in Fig. 18b displays a negative feature curling around the origin. This feature is a transient effect as it is clearly decreasing with time, very likely due to ionic rearrangement at the surface. The TPV signal develops an initial negative spike as shown in Fig. 19c. Fig. 19d compares the evolution of both negative signals. For IMVS, it is taken the magnitude of the negative arc crossing the real axis, normalized to the initial value. For TPV, the amplitude of the negative inflection point of the transient response is plotted, again normalized to the initial value. Excellent agreement can be seen between these two different measurements, which provides evidence that the true IMVS response at high frequency has been measured. Further interpretation of negative spikes has been described recently.[68]

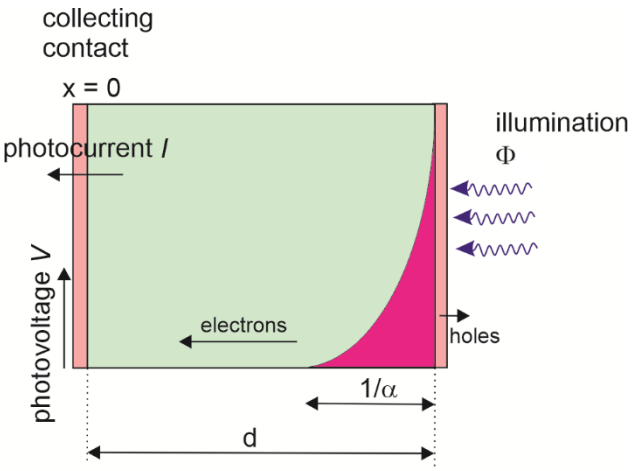

Fig. 20. Scheme of the IMPS and IMVS measurement of a solar cell. Here the illuminated side ($x = d$) is the selective contact for holes, and the photogenerated electrons travel by diffusion to the other electrode ($x = 0$) where current and voltage are measured. Reproduced from [71]. Copyright (2021) American Chemical Society.

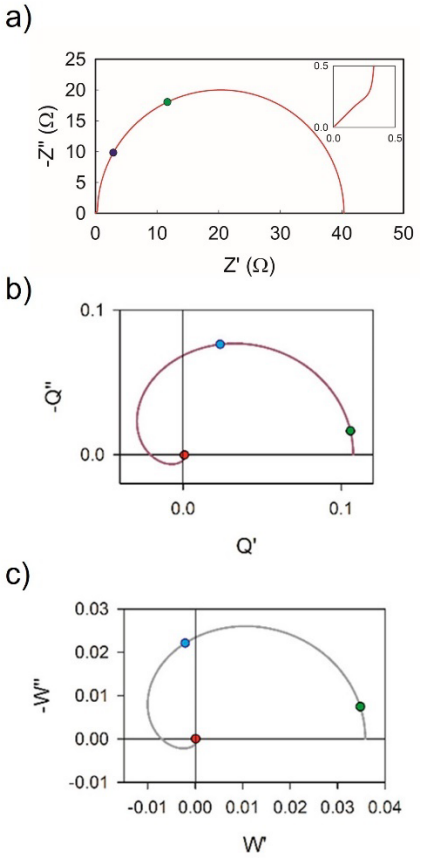

Figure 21. (a) IS, (b) IMPS and (c) IMVS spectra for typical values of a carbon-based perovskite solar cell. The values of the parameters are $R_d = 1\Omega$, $\omega_d = 1.2 \times 10^5\ s^{-1}$ (green), $\omega_\alpha = 1 \times 10^5\ s^{-1}$ (red), and $\omega_{rec} = 5 \times 10^4\ s^{-1}$ (blue). The inset in (a) shows the IS spectrum at high frequency. Reproduced from Ref. [72]. Copyright: The authors of Ref. [72].

Recently it was observed that IMPS spectra show negative values at high frequency, especially occurring in long halide perovskite cells, such as the carbon cell reported in Fig. 17b. It was shown[71] that such negative value is a feature of the diffusion-recombination model,[73,74] that can be formulated as

$$\frac{\partial n}{\partial t} = D_n \frac{\partial^2 n}{\partial x^2} - \frac{n - n_0}{\tau_n} + \alpha \Phi(t) e^{\alpha(x-d)} \tag{30}$$

Here, D_n is the diffusion coefficient, n_0 the equilibrium density under dark conditions, τ_n the recombination lifetime, d the solar cell thickness, and α the light absorption coefficient. A scheme of the model showing the spatial distribution of charge is indicated in Fig. 20. By solving the transfer functions, we obtain the following forms according to the three characteristic frequencies indicated in Table 2, namely $\omega_{rec}, \omega_d, \omega_\alpha$.[8,72] For IS

$$Z(\omega) = R_d \left(\frac{\omega_d}{p}\right)^{1/2} coth\left(\left(\frac{p}{\omega_d}\right)^{1/2}\right) \tag{31}$$

where R_d is the diffusion resistance, and p is defined as

$$p = i\omega + \omega_{rec} \tag{32}$$

For IMPS

$$Q(\omega) = \frac{F(\omega)}{\cosh\left[\left(\frac{p}{\omega_d}\right)^{1/2}\right]} \tag{33}$$

and for IMVS

$$W(\omega) = R_d \frac{F(\omega)}{\left(\frac{p}{\omega_d}\right)^{1/2} \sinh\left[\left(\frac{p}{\omega_d}\right)^{1/2}\right]} \tag{34}$$

The transfer functions of IMPS and IMVS have a common factor $F(\omega)$ that is defined as

$$F(\omega) = \frac{1 - e^{-\alpha d}\left\{e^{(p/\omega_d)^{1/2}} + \left[\left(\frac{p}{\omega_\alpha}\right)^{1/2} - 1\right]\sinh\left[\left(\frac{p}{\omega_d}\right)^{1/2}\right]\right\}}{\left[1 - \frac{p}{\omega_\alpha}\right]} \tag{35}$$

Note that Q_0, the low frequency value of IMPS, depends on the series resistance, not included in Eq. (30), and on the absorptance of the sample.[8,69]

A representation of the spectra is shown in Fig. 21. We observe that the negative feature of IMPS and IMVS contains direct information on the recombination lifetime, since ω_{rec} can be identified with good spectral resolution at high frequency, quite apart from the ionic distortions that occur at low frequency as indicated in Fig. 17. The method has been shown experimentally to provide the lifetime and diffusion coefficient in different experimental configurations.[71] However, this method requires that the light penetration distance is short, as indicated in Fig. 20. It is complementary to those explained in previous sections, but it comes at the price on inducing highly nonhomegenous conditions of carrier density.

Table 2: Characteristic frequencies of the generation-diffusion recombination system and their relationships

$\omega_{rec} = {\tau_n}^{-1}$	Recombination
$\omega_d = \frac{D_n}{d^2}$	Diffusion over the cell thickness d
$\omega_\alpha = D_n \alpha^2$	Diffusion over light absorption distance
$\frac{\omega_d}{\omega_{rec}} = \left(\frac{L_n}{d}\right)^2$	Diffusion length to film size
$\frac{\omega_\alpha}{\omega_d} = (\alpha d)^2$	Film size to light absorption length

$\frac{\omega_\alpha}{\omega_{rec}} = (\alpha L_n)^2$	Diffusion length to absorption length

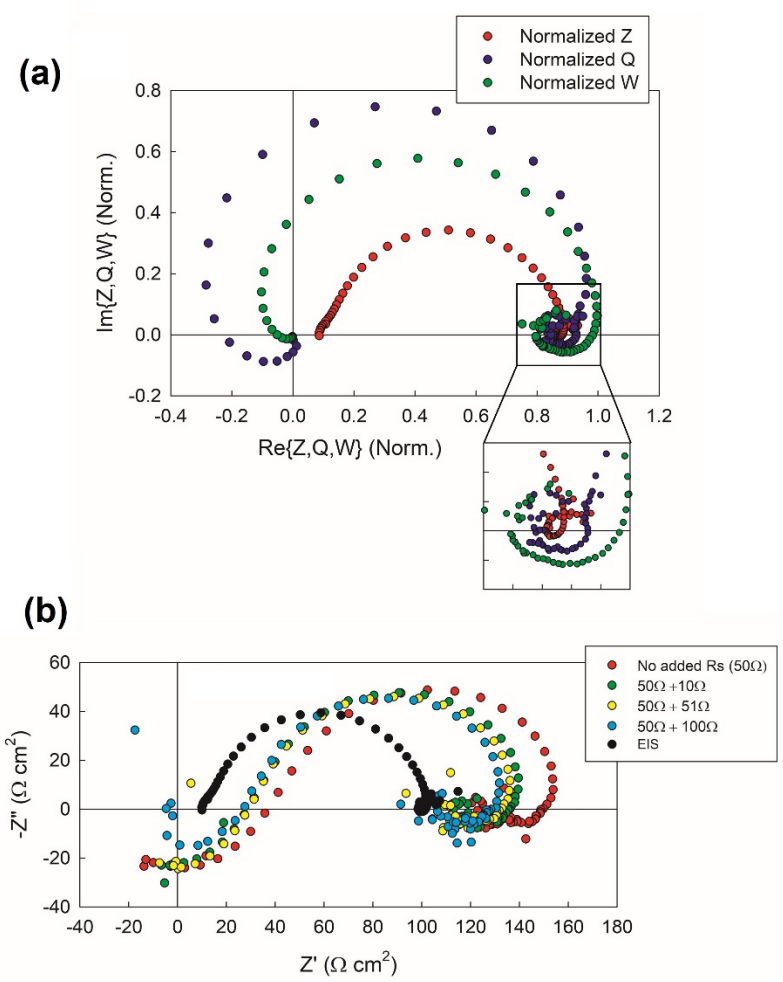

Figure 22. Experimental complex plane plots of the IS, IMPS and IMVS for a carbon-based perovskite solar cell. (a) shows the three normalized spectra together. (b) Experimental complex plane plots of the directly measured IS (black points) and the experimental quotient of IMPS and IMVS given by Eq. (28). Reproduced from Ref. [72]. Copyright: The authors of Ref. [72].

Fig. 22 shows the measurement of the three transfer functions of IS, IMPS and IMVS for a carbon-based perovskite solar cell.[72] The experimental spectra in Fig. 22a show the shapes of the model in Fig. 21. It is noticed that the IMPS and IMVS show the diffusional negative part, while the IS shows only positive values. The reason for this is that the light generation produces information included in the factor of Eq. (34) that is present in both IMVS and IMPS, but not in IS. The factor disappears when calculating the impedance in Eq. (31) by the division of Eq. (29), $Z = W/Q$.

Fig. 22b shows the experimental realization of the division of IMVS and IMPS data. It is confirmed that the negative parts of Q and W cancel out leaving only positive values for Z. Going back to Fig. 17, we note that IMPS contains a real negative part but IMVS does not. This is inconsistent as we have observed in Fig. 22, and it has to be attributed to an experimental error of the measurement of W at high frequency. Such defect is resolved in the experimental setup developed by Adam Pockett,[70,72] as shown by the positive answer to consistency tests that has ben obtained in Fig. 19 and Fig. 22.

In summary it is found that the light-modulated techniques contain information that is not present in IS.

In conclusion, a variety of methods allow to measure the response time in optoelectronic devices with contacts, using a combination of physical signals based on light absorption and emission, voltage and current. Such response times need a suitable interpretation that we have provided here in terms of RC products based on the equivalent circuit model of any small perturbation method over a stabilized stationary state. The identification of the recombination lifetime is based on the criterion that the chemical capacitance and the recombination resistance are clearly observed. In the field of halide perovskites there have been reports of the lifetime dependence on the internal voltage. However the interpretation of capacitances and recombination resistances is still an issue that requires further investigation. The consistency of different methods: IS, IMVS, IMPS, TPV, is an important tool to establish the intrinsic dynamic properties. In the case of elementary decay models all techniques give the answer. We showed that in more complex multicomponent samples or in nonhomogeneous conditions, the different methods are consistent but they may show different pieces of information about the sample behaviour.

Acknowledgments

We thank the financial support by the Ministerio de Ciencia e Innovación of Spain (MICINN) project PID2019-107348GB-100.

References

(1) Bisquert, J. *The Physics of Solar Energy Conversion*; CRC Press: Boca Raton, 2020.

(2) Kirchartz, T.; Márquez, J. A.; Stolterfoht, M.; Unold, T. Photoluminescence-Based Characterization of Halide Perovskites for Photovoltaics, *Adv. Energy Mater.* **2020**, *10*, 1904134.

(3) Staub, F.; Hempel, H.; Hebig, J.-C.; Mock, J.; Paetzold, U. W.; Rau, U.; Unold, T.; Kirchartz, T. Beyond Bulk Lifetimes: Insights into Lead Halide Perovskite Films from Time-Resolved Photoluminescence, *Phys. Rev. Appl.* **2016**, *6*, 044017.

(4) Wolff, C. M.; Caprioglio, P.; Stolterfoht, M.; Neher, D. Nonradiative Recombination in Perovskite Solar Cells: The Role of Interfaces, *Adv. Mater.* **2019**, *31*, 1902762.

(5) Correa-Baena, J.-P.; Turren-Cruz, S.-H.; Tress, W.; Hagfeldt, A.; Aranda, C.; Shooshtari, L.; Bisquert, J.; Guerrero, A. Changes from Bulk to Surface Recombination Mechanisms between Pristine and Cycled Perovskite Solar Cells, *ACS Energy Lett.* **2017**, 681-688.

(6) Zaban, A.; Greenshtein, M.; Bisquert, J. Determination of the electron lifetime in nanocrystalline dye solar cells by open-circuit voltage decay measurements, *ChemPhysChem* **2003**, *4*, 859-864.

(7) Baumann, A.; Tvingstedt, K.; Heiber, M. C.; Vath, S.; Momblona, C.; Bolink, H. J.; Dyakonov, V. Persistent photovoltage in methylammonium lead iodide perovskite solar cells, *APL Materials* **2014**, *2*, 081501.

(8) Bisquert, J.; Janssen, M. From Frequency Domain to Time Transient Methods for Halide Perovskite Solar Cells: The Connections of IMPS, IMVS, TPC and TPV, *J. Phys. Chem. Lett.* **2021**, *12*, 7964–7971.

(9) Guerrero, A.; Bisquert, J.; Garcia-Belmonte, G. Impedance spectroscopy of metal halide perovskite solar cells from the perspective of equivalent circuits, *Chemical Reviews* **2021**, *121*, 14430–14484.

(10) Mora-Seró, I.; Garcia-Belmonte, G.; Boix, P. P.; Vázquez, M. A.; Bisquert, J. Impedance characterisation of highly efficient silicon solar cell under different light illumination intensities *Energy Environ. Sci.* **2009**, *2*, 678–686.

(11) Péan, E. V.; Dimitrov, S.; De Castro, C. S.; Davies, M. L. Interpreting time-resolved photoluminescence of perovskite materials, *Phys. Chem. Chem. Phys.* **2020**, *22*, 28345-28358.

(12) Maurano, A.; Hamilton, R.; Shuttle, C. G.; Ballantyne, A. M.; Nelson, J.; O'Regan, B.; Zhang, W.; McCulloch, I.; Azimi, H.; Morana, M.; Brabec, C. J.; Durrant, J. R. Recombination Dynamics as a Key Determinant of Open Circuit Voltage in Organic

Bulk Heterojunction Solar Cells: A Comparison of Four Different Donor Polymers, *Adv. Mater.* **2010**, *22*, 4987-4992.

(13) Bisquert, J. ; Zaban, A.; Greenshtein, M.; Mora-Seró, I. Determination of rate constants for charge transfer and the distribution of semiconductor and electrolyte electronic energy levels in dye-sensitized solar cells by open-circuit photovoltage decay method., *J. Am. Chem. Soc.* **2004**, *126*, 13550.

(14) Kiermasch, D.; Baumann, A.; Fischer, M.; Dyakonov, V.; Tvingstedt, K. Revisiting lifetimes from transient electrical characterization of thin film solar cells; a capacitive concern evaluated for silicon, organic and perovskite devices, *Energy Environ. Sci.* **2018**, *11*, 629-640.

(15) Wolff, C. M.; Bourelle, S. A.; Phuong, L. Q.; Kurpiers, J.; Feldmann, S.; Caprioglio, P.; Marquez, J. A.; Wolansky, J.; Unold, T.; Stolterfoht, M.; Shoaee, S.; Deschler, F.; Neher, D. Orders of Recombination in Complete Perovskite Solar Cells – Linking Time-Resolved and Steady-State Measurements, *Adv. Energy Mater.* **2021**, *11*, 2101823.

(16) Krückemeier, L.; Liu, Z.; Krogmeier, B.; Rau, U.; Kirchartz, T. Consistent Interpretation of Electrical and Optical Transients in Halide Perovskite Layers and Solar Cells, *Adv. Energy Mater.* **2021**, *11*, 2102290.

(17) Almora, O.; Garcia-Belmonte, G. Light capacitances in silicon and perovskite solar cells, *Sol. Ener.* **2019**, *189*, 103-110.

(18) Bisquert, J.; Garcia-Belmonte, G.; Mora-Sero, I. Characterization of Capacitance, Transport and Recombination Parameters in Hybrid Perovskite and Organic Solar Cells. In *Unconventional Thin Film Photovoltaics* Como, E. D., Angelis, F. D., Snaith, H., Walker, A., Eds.; Royal Society of Chemistry, 2016.

(19) Rose, A. *Concepts in Photoconductivity and Allied Problems*; Interscience: New York, 1963.

(20) Mora-Seró, I.; Luo, Y.; Garcia-Belmonte, G.; Bisquert, J.; Muñoz, D.; Voz, C.; Puigdollers, J.; Alcubilla, R. Recombination rates in heterojunction silicon solar cells analyzed by impedance spectroscopy at forward bias and under illumination, *Sol. En. Mater. Sol. Cell* **2008**, *92*, 505-509.

(21) Credgington, D.; Kim, Y.; Labram, J.; Anthopoulos, T. D.; Durrant, J. R. Analysis of Recombination Losses in a Pentacene/C60 Organic Bilayer Solar Cell, *J. Phys. Chem. Lett.* **2011**, *2*, 2759-2763.

(22) Clarke, T. M.; Lungenschmied, C.; Peet, J.; Drolet, N.; Mozer, A. J. A Comparison of Five Experimental Techniques to Measure Charge Carrier Lifetime in Polymer/Fullerene Solar Cells, *Adv. Energy Mater.* **2015**, *5*, 1401345.

(23) Bisquert, J.; Vikhrenko, V. S. Interpretation of the time constants measured

by kinetic techniques in nanostructured semiconductor electrodes and dye-sensitized solar cells., *J. Phys. Chem. B* **2004**, *108*, 2313-2322.

(24) Bisquert, J.; Fabregat-Santiago, F.; Mora-Seró, I.; Garcia-Belmonte, G.; Giménez, S. Electron lifetime in dye-sensitized solar cells: theory and interpretation of measurements, *J. Phys. Chem. C* **2009**, *113*, 17278–17290.

(25) Bisquert, J.; Marcus, R. A. Device modeling of dye-sensitized solar cells, *Topics in Current Chemistry* **2014**, *352*, 325-396.

(26) Jennings, J. R.; Peter, L. M. A Reappraisal of the Electron Diffusion Length in Solid-State Dye-Sensitized Solar Cells, *J. Phys. Chem. C* **2007**, *111*, 16100-16104.

(27) Bisquert, J. Physical electrochemistry of nanostructured devices, *Phys. Chem. Chem. Phys.* **2008**, *10*, 49-72.

(28) Anta, J. A.; Mora-Seró, I.; Dittrich, T.; Bisquert, J. Interpretation of diffusion coefficients in nanostructured materials from random walk numerical simulation, *Phys. Chem. Chem. Phys.* **2008**, *10*, 4478-4485.

(29) Wang, Z. S.; Ebadi, F.; Carlsen, B.; Choy, W. C. H.; Tress, W. Transient Photovoltage Measurements on Perovskite Solar Cells with Varied Defect Concentrations and Inhomogeneous Recombination Rates, *Small Methods* **2020**, *4*, 2000290.

(30) Tress, W.; Yavari, M.; Domanski, K.; Yadav, P.; Niesen, B.; Correa Baena, J. P.; Hagfeldt, A.; Graetzel, M. Interpretation and evolution of open-circuit voltage, recombination, ideality factor and subgap defect states during reversible light-soaking and irreversible degradation of perovskite solar cells, *Energy Environ. Sci.* **2018**, *11*, 151-165.

(31) Caprioglio, P.; Stolterfoht, M.; Wolff, C. M.; Unold, T.; Rech, B.; Albrecht, S.; Neher, D. On the Relation between the Open-Circuit Voltage and Quasi-Fermi Level Splitting in Efficient Perovskite Solar Cells, *Adv. Energy Mater.* **2019**, *9*, 1901631.

(32) Krückemeier, L.; Krogmeier, B.; Liu, Z.; Rau, U.; Kirchartz, T. Understanding Transient Photoluminescence in Halide Perovskite Layer Stacks and Solar Cells, *Adv. Energy Mater.* **2021**, *11*, 2003489.

(33) Johnston, M. B.; Herz, L. M. Hybrid Perovskites for Photovoltaics: Charge-Carrier Recombination, Diffusion, and Radiative Efficiencies, *Acc. Chem. Res.* **2016**, *49*, 146-154.

(34) Bisquert, J. Chemical capacitance of nanostructured semiconductors: its origin and significance for heterogeneous solar cells, *Phys. Chem. Chem. Phys.* **2003**, *5*, 5360-5364.

(35) Garcia-Belmonte, G.; García-Cañadas, J.; Mora-Seró, I.; Bisquert, J.; Voz, C.; Puigdollers, J.; Alcubilla, R. Effect of buffer layer on minority carrier lifetime and

series resistance of bifacial heterojunction silicon solar cells analyzed by impedance spectroscopy, *Thin Solid Films* **2006**, *514*, 254–257.

(36) Almora, O.; Gerling, L. G.; Voz, C.; Alcubilla, R.; Puigdollers, J.; Garcia-Belmonte, G. Superior performance of V2O5 as hole selective contact over other transition metal oxides in silicon heterojunction solar cells, *Sol. En. Mater. Sol. Cell* **2017**, *168*, 221-226.

(37) Chouffot, R.; Ibrahim, S.; Brüggemann, R.; Gudovskikh, A. S.; Kleider, J. P.; Scherff, M.; Fahrner, W. R.; Cabarrocas, P. R. i.; Eon, D.; Ribeyron, P. J. Comparison of photoluminescence and capacitance spectroscopies as efficient tools for interface characterisation of heterojunction solar cells, *Journal of Non-Crystalline Solids* **2008**, *354*, 2416-2420.

(38) Wang, Q.; Ito, S.; Grätzel, M.; Fabregat-Santiago, F.; Mora-Seró, I.; Bisquert, J.; Bessho, T.; Imai, H. Characteristics of high efficiency dye-sensitized solar cells, *J. Phys. Chem. B* **2006**, *110*, 19406-19411.

(39) Fabregat-Santiago, F.; Garcia-Belmonte, G.; Mora-Seró, I.; Bisquert, J. Characterization of nanostructured hybrid and organic solar cells by impedance spectroscopy, *Phys. Chem. Chem. Phys.* **2011**, *13*, 9083–9118.

(40) Garcia-Belmonte, G.; Boix, P. P.; Bisquert, J.; Lenes, M.; Bolink, H. J.; La Rosa, A.; Filippone, S.; Martín, N. Influence of the intermediate density-of-states occupancy on open-circuit voltage of bulk heterojunction solar cells with different fullerene acceptors, *J. Phys. Chem. Lett.* **2010**, *1*, 2566–2571.

(41) Ravishankar, S.; Bisquert, J.; Kirchartz, T. Interpretation of Mott–Schottky plots of photoanodes for water splitting, *Chemical Science* **2022**, *13*, 4828-4837.

(42) Wheeler, S.; Bryant, D.; Troughton, J.; Kirchartz, T.; Watson, T.; Nelson, J.; Durrant, J. R. Transient Optoelectronic Analysis of the Impact of Material Energetics and Recombination Kinetics on the Open-Circuit Voltage of Hybrid Perovskite Solar Cells, *J. Phys. Chem. C* **2017**, *121*, 13496-13506.

(43) Almora, O.; Cho, K. T.; Aghazada, S.; Zimmermann, I.; Matt, G. J.; Brabec, C. J.; Nazeeruddin, M. K.; Garcia-Belmonte, G. Discerning recombination mechanisms and ideality factors through impedance analysis of high-efficiency perovskite solar cells, *Nano Energy* **2018**, *48*, 63-72.

(44) Bisquert, J.; Guerrero, A.; Gonzales, C. Theory of Hysteresis in Halide Perovskites by Integration of the Equivalent Circuit, *ACS Phys. Chem Au* **2021**, *1*, 25-44.

(45) Neukom, M. T.; Schiller, A.; Züfle, S.; Knapp, E.; Ávila, J.; Pérez-del-Rey, D.; Dreessen, C.; Zanoni, K. P. S.; Sessolo, M.; Bolink, H. J.; Ruhstaller, B. Consistent Device Simulation Model Describing Perovskite Solar Cells in Steady-State, Transient, and Frequency Domain, *ACS Appl. Mat. Int.* **2019**, *11*, 23320-23328.

(46) Zarazua, I.; Han, G.; Boix, P. P.; Mhaisalkar, S.; Fabregat-Santiago, F.; Mora-Seró, I.; Bisquert, J.; Garcia-Belmonte, G. Surface Recombination and Collection Efficiency in Perovskite Solar Cells from Impedance Analysis, *J. Phys. Chem. Lett.* **2016**, *7*, 5105-5113.

(47) Hernández-Balaguera, E.; Romero, B.; Najafi, M.; Galagan, Y. Analysis of Light-Enhanced Capacitance Dispersion in Perovskite Solar Cells, *Advanced Materials Interfaces* **2022**, *9*, 2102275.

(48) von Hauff, E.; Klotz, D. Impedance spectroscopy for perovskite solar cells: characterisation, analysis, and diagnosis, *J. Mat. Chem. C* **2022**, *10*, 742-761.

(49) Almora, O.; Aranda, C.; Garcia-Belmonte, G. Do Capacitance Measurements Reveal Light-Induced Bulk Dielectric Changes in Photovoltaic Perovskites?, *J. Phys. Chem. C* **2018**, *122*, 13450-13454.

(50) Guerrero, A.; Garcia-Belmonte, G.; Mora-Sero, I.; Bisquert, J.; Kang, Y. S.; Jacobsson, T. J.; Correa-Baena, J.-P.; Hagfeldt, A. Properties of Contact and Bulk Impedances in Hybrid Lead Halide Perovskite Solar Cells Including Inductive Loop Elements, *J. Phys. Chem. C* **2016**, *120*, 8023-8032.

(51) Bou, A.; Pockett, A.; Raptis, D.; Watson, T.; Carnie, M. J.; Bisquert, J. Beyond Impedance Spectroscopy of Perovskite Solar Cells: Insights from the Spectral Correlation of the Electrooptical Frequency Techniques, *J. Phys. Chem. Lett.* **2020**, *11*, 8654-8659.

(52) Pockett, A.; Eperon, G. E.; Sakai, N.; Snaith, H. J.; Peter, L. M.; Cameron, P. J. Microseconds, milliseconds and seconds: deconvoluting the dynamic behaviour of planar perovskite solar cells, *Phys. Chem. Chem. Phys.* **2017**, *19*, 5959-5970.

(53) Yoo, S.-M.; Yoon, S. J.; Anta, J. A.; Lee, H. J.; Boix, P. P.; Mora-Seró, I. An Equivalent Circuit for Perovskite Solar Cell Bridging Sensitized to Thin Film Architectures, *Joule* **2019**, *3*, 2535-2549.

(54) van Roosbroeck, W.; Casey, H. C., Jr. Transport in Relaxation Semiconductors, *Phys. Rev. B* **1972**, *5*, 2154-2175.

(55) Wang, H.; Guerrero, A.; Bou, A.; Al-Mayouf, A. M.; Bisquert, J. Kinetic and material properties of interfaces governing slow response and long timescale phenomena in perovskite solar cells, *Energy Environ. Sci.* **2019**, *12*, 2054-2079.

(56) Chouffot, R.; Brezard-Oudot, A.; Kleider, J. P.; Brüggemann, R.; Labrune, M.; Roca i Cabarrocas, P.; Ribeyron, P. J. Modulated photoluminescence as an effective lifetime measurement method: Application to a-Si:H/c-Si heterojunction solar cells, *Materials Science and Engineering: B* **2009**, *159–160*, 186-189.

(57) Schlichthörl, G.; Huang, S. Y.; Sprague, J.; Frank, A. J. Band edge movement and recombination kinetics in dye-sensitized nanocrystalline TiO2 solar cells:

a study by intensity modulated photovoltage spectroscopy, *J. Phys. Chem. B* **1997**, *101*, 8141-8155.

(58) Correa-Baena, J.-P.; Tress, W.; Domanski, K.; Anaraki, E. H.; Turren-Cruz, S.-H.; Roose, B.; Boix, P. P.; Grätzel, M.; Saliba, M.; Abate, A.; Hagfeldt, A. Identifying and suppressing interfacial recombination to achieve high open-circuit voltage in perovskite solar cells, *Energy Environ. Sci.* **2017**, *10*, 1207-1212.

(59) Nurunnizar, A. A.; Wulandari, P.; Bahar, H.; Fitrilawati, F.; Khalil, M.; Hidayat, R. The influences of interfacial recombination loss on the perovskite solar cell performance studied by transient photovoltage spectroscopy, *Materials Science in Semiconductor Processing* **2021**, *135*, 106095.

(60) Ravishankar, S.; Aranda, C.; Sanchez, S.; Bisquert, J.; Saliba, M.; Garcia-Belmonte, G. Perovskite Solar Cell Modeling Using Light and Voltage Modulated Techniques, *J. Phys. Chem. C* **2019**, *123*, 6444-6449.

(61) Pockett, A.; Eperon, G. E.; Peltola, T.; Snaith, H. J.; Walker, A. B.; Peter, L. M.; Cameron, P. J. Characterization of planar lead halide perovskite solar cells by impedance spectroscopy, open circuit photovoltage decay and intensity-modulated photovoltage/photocurrent spectroscopy, *J. Phys. Chem. C* **2015**, *119*, 3456–3465.

(62) Riquelme, A.; Gálvez, F. E.; Contreras-Bernal, L.; Míguez, H.; Anta, J. A. Internal quantum efficiency and time signals from intensity-modulated photocurrent spectra of perovskite solar cells, *J. Appl. Phys.* **2020**, *128*, 133103.

(63) Parikh, N.; Narayanan, S.; Kumari, H.; Prochowicz, D.; Kalam, A.; Satapathi, S.; Akin, S.; Tavakoli, M. M.; Yadav, P. Recent Progress of Light Intensity-Modulated Small Perturbation Techniques in Perovskite Solar Cells, *physica status solidi (RRL) – Rapid Research Letters* **2021**, *n/a*, 2100510.

(64) Bertoluzzi, L.; Bisquert, J. Investigating the Consistency of Models for Water Splitting Systems by Light and Voltage Modulated Techniques, *J. Phys. Chem. Lett.* **2017**, *8*, 172-180.

(65) Mei, A.; Li, X.; Liu, L.; Ku, Z.; Liu, T.; Rong, Y.; Xu, M.; Hu, M.; Chen, J.; Yang, Y.; Grätzel, M.; Han, H. A hole-conductor–free, fully printable mesoscopic perovskite solar cell with high stability, *Science* **2014**, *345*, 295.

(66) Bisquert, J.; Guerrero, A. Chemical Inductor, *J. Am. Chem. Soc.* **2022**, *144*, 5996–6009.

(67) Berruet, M.; Pérez-Martínez, J. C.; Romero, B.; Gonzales, C.; Al-Mayouf, A. M.; Guerrero, A.; Bisquert, J. Physical model for the current-voltage hysteresis and impedance of halide perovskite memristors, *ACS Energy Lett.* **2022**, *7*, 1214–1222.

(68) Hernández-Balaguera, E.; Bisquert, J. Negative Transient Spikes in Halide Perovskites, *ACS Energy Lett.* **2022**, 2602-2610.

(69) Alvarez, A. O.; Ravishankar, S.; Fabregat-Santiago, F. Combining Modulated Techniques for the Analysis of Photosensitive Devices, *Small Methods* **2021**, *n/a*, 2100661.

(70) Pockett, A.; Spence, M.; Thomas, S. K.; Raptis, D.; Watson, T.; Carnie, M. J. Beyond the First Quadrant: Origin of the High Frequency Intensity-Modulated Photocurrent/Photovoltage Spectroscopy Response of Perovskite Solar Cells, *Solar RRL* **2021**, *5*, 2100159.

(71) Bou, A.; Āboliņš, H.; Ashoka, A.; Cruanyes, H.; Guerrero, A.; Deschler, F.; Bisquert, J. Extracting in Situ Charge Carrier Diffusion Parameters in Perovskite Solar Cells with Light Modulated Techniques, *ACS Energy Lett.* **2021**, 2248-2255.

(72) Bou, A.; Pockett, A.; Cruanyes, H.; Raptis, D.; Watson, T.; Carnie, M. J.; Bisquert, J. Limited information of impedance spectroscopy about electronic diffusion transport: The case of perovskite solar cells, *APL Materials* **2022**, *10*, 051104.

(73) Dloczik, L.; Ileperuma, O.; Lauerman, I.; Peter, L. M.; Ponomarev, E. A.; Redmond, G.; Shaw, N. J.; Uhlendorf, I. Dynamic Response of Dye-Sensitized Nanocrystalline Solar Cells: Characterization by Intensity-Modulated Photocurrent Spectroscopy, *J. Phys. Chem. B* **1997**, *101*, 10281-10289.

(74) Halme, J.; Miettunen, K.; Lund, P. Effect of Nonuniform Generation and Inefficient Collection of Electrons on the Dynamic Photocurrent and Photovoltage Response of Nanostructured Photoelectrodes, *J. Phys. Chem. C* **2008**, *112*, 20491-20504.